

Effect of an Inserted Porous Layer Located at a Wall of a Parallel Plate Channel on Forced Convection Heat Transfer

Eren Ucar · Moghtada Mobedi · Ioan Pop

Received: 8 October 2012 / Accepted: 25 January 2013 / Published online: 14 February 2013
© Springer Science+Business Media Dordrecht 2013

Abstract A theoretical study is performed on heat and fluid flow in partially porous medium filled parallel plate channel. A uniform symmetrical heat flux is imposed onto the boundaries of the channel partially filled with porous medium. The dimensional forms of the governing equations are solved numerically for different permeability and effective thermal conductivity ratios. Then, the governing equations are made dimensionless and solved analytically. The results of two approaches are compared and an excellent agreement is observed, indicating correctness of the both solutions. An overall Nusselt number is defined based on overall thermal conductivity and difference between the average temperature of walls and mean temperature to compare heat transfer in different channels with different porous layer thickness, Darcy number, and thermal conductivity ratio. Moreover, individual Nusselt numbers for upper and lower walls are also defined and obtained. The obtained results show that the maximum overall Nusselt number is achieved for thermal conductivity ratio of 1. At specific values of Darcy number and thermal conductivity ratio, individual Nusselt numbers approach to infinity since the value of wall temperatures approaches to mean temperature.

Keywords Porous medium · Partially filled porous media · Channel flow · Fully developed.

List of Symbols

Da	Darcy number
f	Friction coefficient
G	Pressure gradient in x - direction
h	Convective heat transfer coefficient, W/m ² K
H	Half height of channel

E. Ucar · M. Mobedi

Mechanical Engineering Department, Izmir Institute of Technology, 35430 Urla, Izmir, Turkey

I. Pop (✉)

Department of Mathematics, Babeş -Bolyai University, 40084 Cluj-Napoca, Romania

e-mail: popm.ioan@yahoo.co.uk

k_m	The overall thermal conductivity, W/m K
K	Permeability, m^2
K^*	The ratio of effective conductivity over fluid conductivity
L	Length of the channel, m
M	Dimensionless viscosity ratio parameter
Nu_m	Overall Nusselt number
Re	Reynolds number
q''	heat flux, W/m^2
S	Porous media shape parameter
T	Temperature, K
T_i	Initial temperature, K
u	Velocity component along x - direction, m/s
U	Dimensionless velocity component along dimensionless X - direction, m/s
U_i	Dimensionless interface velocity component along dimensionless X - direction
\hat{u}	Dimensionless normalized velocity
x	Coordinate along the axis of the channel, m
y	Coordinate normal to the surfaces of the channel, m
X, Y	Dimensionless coordinates

Greek letters

β	Coefficient for the walls
ε	Porosity
μ	Dynamic viscosity, kg/m s
ν	Kinematic viscosity of fluid, m^2/s
θ	Dimensionless temperature
θ_i	The dimensionless interface temperature
ρ	Density, kg/m^3
ξ	Porous thickness

Subscripts

c	Clear fluid region
eff	Effective
f	Fluid
m	Mean
p	Porous
r	Ratio
s	Solid
t	Total
w	Wall
wu	Upper wall
wl	Lower wall
$w \mu$	Average wall
u	Belongs to the upper wall
l	Belongs to the lower wall

1 Introduction

The use of porous media to improve forced convection heat transfer in channels has taken attention of researchers in recent years. Numerical and experimental studies on internal flows in a channel or duct have been examined to provide a deeper understanding of the transport mechanism of momentum and heat through partially or fully filled porous medium channels. Completely porous medium-filled channel may be penalized by increasing pressure drop which in turns increases the cost of the pumping work. Therefore, partially porous medium-filled channel may be an alternative way to reduce the increment of pressure drop.

A considerable number of investigations on forced convection in partially filled porous channel and ducts have been performed and reported in literature. The summary of those studies are shown in the Table 1 to simplify comprehension of the problems according to the dimensions, governing equations, outer surface thermal conditions, and solution methods. The schematic views of the studies are also given in the table. [Poulikakos and Kazmierczak \(1987\)](#) investigated the problem of forced convection in a duct partially filled with a porous medium, analytically and numerically. They used two channel geometries as parallel plates and circular ducts and two types of boundary conditions as constant heat flux and constant wall temperature. The Brinkman extended Darcy model was used to describe the flow within the porous material. The study states that the dependence of the Nusselt number on the thickness of the porous region is not uniform, so they found a thickness at which the Nusselt number value reaches minimum. [Al-Nimr and Alkam \(1997\)](#) employed a porous substrate in a tubeless solar collector to improve the convective heat transfer between the absorber plate and the fluid. The collector efficiency had been improved by 3–32 % under favor of porous substance. They stated that there is an optimum porous substrate thickness beyond which the collector efficiency does not considerably change due to the increase of pressure drop. Pulsating flow and heat transfer in a channel, the walls of which were layered by a porous medium, were considered by [Guo et al. \(1997\)](#) for constant heat flux thermal condition on the outer surface. The Brinkman-Forcheimer extended Darcy model was used to obtain velocity profile in the channel. The study focuses on the effects of pulsation in partially filled channel and an optimum porous layer thickness for the maximum effective thermal diffusivity.

[Kuznetsov \(1998, 1999\)](#) investigated the problem of forced convection partially porous medium filled channel with Couette flow. Kuznetsov used the Brinkman-Forcheimer extended Darcy model and obtain analytical expressions for velocity and temperature distributions. Different thermal boundary conditions for Couette flow were studied and the expressions for velocity and temperature profiles were obtained. The influence of Da number on the velocity profile and Nu number were discussed. An analytical investigation for the channel which is partially filled by bidisperse porous medium was presented by [Kuznetsov and Nield \(2010\)](#). One side of the channel is filled with porous layer while fluid flow in the other side. The effects of thermal conductivity ratio, velocity ratio, volume fraction, internal heat exchange parameter, and the position of the porous-fluid interface on to the Nusselt number were investigated for both symmetrical and asymmetrical heat flux boundary conditions. A singular behavior of the Nusselt number was observed for the case with asymmetric boundary condition. An analysis for fully developed steady state of forced convection in a parallel plate channel partly occupied by porous medium was made by [Nield and Kuznetsov \(2011\)](#). The porous layer is located at the center of channel and lateral boundaries. The authors investigated the change of Nu number according to the predetermined criteria such as thermal conductivity ratio, thickness of porous medium, the interface position, etc. They showed that Nusselt number is strongly affected from the thickness of porous layer and thermal conductivity ratio rather than the other parameters.

Table 1 The summary of reported studies on partially filled channel


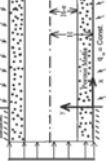
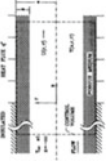
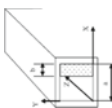
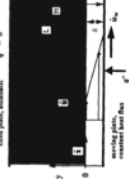
Authors	Dimension	Governing equations	Outer surfaces thermal condition	Interface condition (velocity and thermal)	Solution method	Figure of studied channel/duct
Al-Nimr and Alkam (1997)	2D Cartesian coordinate system	Brinkman Forchheimer extended Darcy	Upper plate subjected to a constant heat flux	Continuity of shear stress and heat flux	Numerical	
Forooghi et al. (2010)	2D Cartesian coordinate system	Brinkman Forchheimer extended Darcy	Constant heat flux on both walls	Continuity of shear stress and a new B.C. is derived	Numerical	
Guo et al. (1997)	2D Cylindrical coordinate system	Brinkman Forchheimer extended Darcy	Constant heat flux	Continuity of shear stress and heat flux	Numerical	
Jen and Yan (2005)	3D Cartesian coordinate system	Complete momentum equations	Constant wall temperature on all walls	Continuity of shear stress and heat flux	Numerical	
Kuznetsov (1998)	2D Cartesian coordinate system	Brinkman Forchheimer extended Darcy	Moving plate is subject to a uniform heat flux The fixed plate is adiabatic.	B-J model continuity of heat flux	Analytical	

Table 1 continued

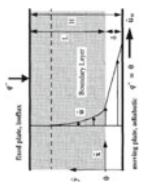
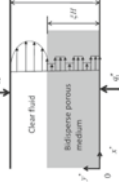

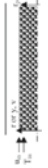
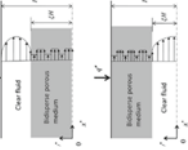
Authors	Dimension	Governing equations	Outer surfaces thermal condition	Interface condition (velocity and thermal)	Solution method	Figure of studied channel/duct
Kuznetsov (1999)	2D Cartesian coordinate system	Brinkman Forchheimer extended Darcy	Moving plate is adiabatic. The fixed plate is subject to a uniform heat flux	B-J model continuity of heat flux	Analytical	
Kuznetsov and Nield (2010)	2D Cartesian coordinate system	Darcy's Law	Constant heat flux on both walls	B-J model and variable Porosity model	Analytical	
Mohamad (2003)	2D Cartesian coordinate system and cylindrical coordinate system	Brinkman Forchheimer extended Darcy	Constant wall temperature	Continuity of shear stress and heat flux	Numerical analytical Eq. given (No solutions)	
Morosuk (2005)	2D Cylindrical coordinate system	Brinkman Forchheimer extended Darcy	Constant wall temperature	Continuity of shear stress and heat flux	Analytical and numerical	
Nield and Kuznetsov (2011)	2D Cartesian coordinate system	Darcy's Law	Constant heat flux on both walls	B-J Model and variable porosity model	Analytical	

Table 1 continued

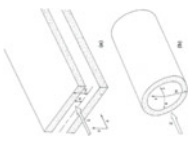


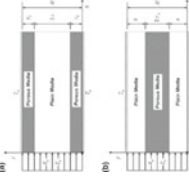
Authors	Dimension	Governing equations	Outer surfaces thermal condition	Interface condition (velocity and thermal)	Solution method	Figure of studied channel/duct
Poulikakos and Kazmierczak (1987)	2D Cartesian coordinate system and cylindrical coordinate system	Brinkman extended Darcy	Constant heat flux and constant wall temperature	Continuity of shear stress and heat flux	Analytical and numerical	
Satyamurty and Bhargavi (2010)	2D Cartesian coordinate system	Brinkman extended non-Darcy model	Constant wall temperature on both walls	B-J model and continuity of heat flux	Analytical, velocity numerical, temperature	
Sayehvand and Shokouhmand (2006)	2D Cylindrical coordinate system	Brinkman Forchheimer extended Darcy	Constant heat flux	Continuity of shear stress and heat flux	Numerical	
Shokouhmand et al. (2011)	2D Cartesian coordinate system	Brinkman extended Darcy model	Constant wall temperature on both walls	Continuity of shear stress and heat flux	Numerical	

Table 1 continued

Authors	Dimension	Governing equations	Outer surfaces thermal condition	Interface condition (velocity and thermal)	Solution method	Figure of studied channel/duct
Teamah et al. (2011)	2D Cylindrical coordinate system	Brinkman Forchheimer extended Darcy	Constant wall temperature	Continuity of shear stress and heat flux	Numerical	
Yang et al. (2009)	2D Cylindrical coordinate system	Brinkman extended Darcy	Constant heat flux	Continuity of shear stress and heat flux	Analytical and numerical	
Yang et al. (2012)	2D Cylindrical coordinate system	Darcy's Law	Constant heat flux	Continuity of shear stress and heat flux	Analytical	

The optimum porous thickness ratio for partially filled ducts or channels with concerning about pressure drop was obtained by [Mohamad \(2003\)](#). It is stated that the inertia term has significant effect on Nu number, but it is not valid for highly porous domains. The author also studied the relation between the length of developing region and Da number. It was concluded that the flow- developing length is not strong function of Da number. Developing flow characteristics of fluid flow and enhanced heat transfer in a partially filled channel were examined by [Jen and Yan \(2005\)](#). They developed a three dimensional computational model. The authors presented the variation of friction factor and Nusselt number as a function of axial position. Moreover, the authors analyzed the effects of the size of porous layer inside the channel partially filled with porous medium on heat and fluid flow. The effects of porous layer thickness and permeability of layer on the rate of entropy generation in the developing and fully developed region of a partially filled duct were investigated by [Morosuk \(2005\)](#). Morosuk performed analytical and numerical study on entropy generation in a channel and duct the center of which is filled with a porous layer. They concluded that the mechanism of entropy generation is mainly dominated by friction and drag force in the porous medium. A detailed numerical study was performed by [Sayehvand and Shokouhmand \(2006\)](#) on a channel with porous layers on its wall. They studied the effects of thickness of porous layer, Darcy number, and the conductivity ratio. They mainly showed that for highly conducting porous media, heat transfer is systematically augmented independent of Darcy value. [Yang et al. \(2009\)](#) studied about optimum porous fractions for forced convection in a partially filled tube. An expression for the optimal porous core diameter ratio was presented in this study. Steady and pulsatile flow for the local thermal non-equilibrium condition was numerically investigated by [Forooghi et al. \(2010\)](#) for the partially filled duct with center located porous layer. They show that solid to fluid thermal conductivity ratio is very important. As the solid-to- fluid thermal conductivity ratio increases, Nusselt number increases. It is also stated that when the thickness of porous media is very small, Nusselt number is negatively affected by the porous media. [Satyamurty and Bhargavi \(2010\)](#) studied the forced convection in a thermally developing region of a parallel plate channel with one side located porous layer. The walls of the channel are maintained at a constant temperature. It was found that the maximum enhancement in heat transfer occurs at a porous fraction of 0.8 at a Darcy number of 0.001 and the maximum enhancement per unit pressure drop occurs at a porous fraction of 0.7. [Shokouhmand et al. \(2011\)](#) studied the effect of porous insert position on enhanced heat transfer in a parallel plate channel partially filled with a fluid saturated porous medium. Two type of porous insert positions were studied as porous layer was attached to the walls and porous layer oriented at the center of the channel. In this paper, it was found that the pressure loss was higher when the location of the porous media is in the channel core. Recently, [Teamah et al. \(2011\)](#) presented a numerical study on the effect of the shape of the porous layer on heat and fluid flow in a cylindrical duct. The shapes of the porous layer were taken as cylindrical shape placed at the centerline of the pipe, annular shape, and finally a cylindrical shape porous layer was located at the center of pipe but far from the channel inlet. In the study, a critical radius was determined and it was obtained that the pressure drop and Nu number have the highest value when the porous has a cylindrical shape placed at the centerline of the pipe. The conclusion of the study had consistence with the conclusion of the study of [Shokouhmand et al. \(2011\)](#).

In the present study, the forced convection heat transfer enhancement in parallel plate channels partially filled by porous media is investigated both numerically and analytically. The comparison between analytical and numerical results is performed and good agreement is observed. Overall Nusselt number is defined by using the average wall temperature and overall thermal conductivity of the channel. Moreover, the individual Nusselt numbers for

upper and lower walls are defined and found. The variation of overall and individual Nusselt numbers with Darcy number, thermal conductivity ratio, and porous layer thickness are presented graphically and detailed discussion is performed.

2 The Studied Channel

The considered channel is partially filled with porous medium. As it can be seen in Fig. 1, the distance between the plates is $2H$. Porous layer is located on the bottom plate of the channel and the distance between center of the channel and layer of interface is shown by ξH . The value of ξ changes between -1 and $+1$. The porous medium is considered as isotropic with constant permeability of K . An incompressible, hydrodynamically and thermally fully developed and steady flow in a channel bounded by two parallel plates is considered. The flow is laminar and the fluid flowing between the particles of the porous medium is assumed to be Newtonian. The viscous dissipation is neglected and also it is assumed that the temperature gradient in y -direction is much greater than it is in x -direction for the thermally fully developed flow. The upper and lower channel walls are subjected to a symmetric and uniform heat flux as q'' . The radiation effect of heat transfer is neglected. In this study, the results of the dimensionless study are presented for porous medium with viscosity ratio of 1.3.

3 Dimensional Study

3.1 Governing Equations and Boundary Conditions

In the considered channel, there are two regions. Considering Fig. 1, in the upper region, pure fluid flows while in the lower region fluid flows in the voids between particles of the porous media. The flow is unidirectional, parallel to the x -axis, and the y -component of velocity is zero since it is hydrodynamically and thermally fully developed. Brinkman—extended Darcy equation is used to simulate fluid flow in the porous layer. Therefore, the equation of motion for clear fluid region and porous layer can be written as

$$v \frac{\partial^2 u_c}{\partial y^2} - \frac{1}{\rho} \frac{\partial P}{\partial x} = 0 \quad (1)$$

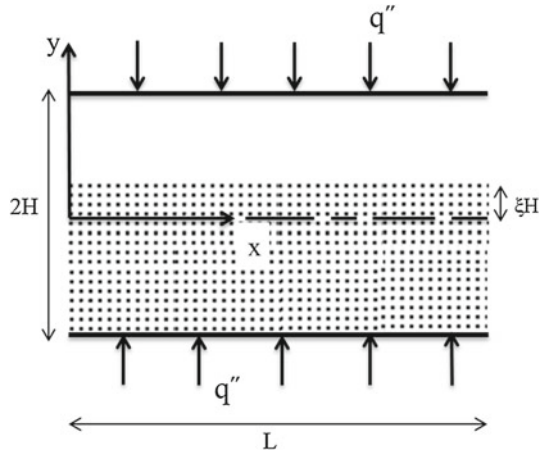
$$\mu_{\text{eff}} \frac{d^2 u_p}{dy^2} - \frac{\mu}{K} u_p - \frac{dP}{dx} = 0 \quad (2)$$

where the letters of u_c and u_p show the fluid velocity in the clear and superficial fluid flow in porous regions, respectively. Considering Fig. 1, the boundary conditions for Eqs. (1) and (2) can be written as

$$\begin{aligned} u_c|_{y=H} &= u_p|_{y=-H} = 0 \\ \mu_f \left. \frac{du_c}{dy} \right|_{y=\xi H} &= \mu_{\text{eff}} \left. \frac{du_p}{dy} \right|_{y=\xi H} \end{aligned} \quad (3)$$

μ_f and μ_{eff} represent the clear fluid and porous region effective dynamic viscosities, respectively. The dynamic viscosity of clear fluid is known since the study is performed for air. The effective dynamic viscosity of porous region can be found from the viscosity ratio (Eq. 8) which is $M=1.3$ for dimensional study. As it is seen from Eq. (3), the continuous shear stress model is used to define boundary condition at the interface between porous layer and clear fluid region. The mean velocity of the fluid in the channel can be calculated by the following definition.

Fig. 1 Schematic view of the considered channel



$$u_{\text{mean}} = \frac{\int_{-H}^{\xi H} u_p dy + \int_{\xi H}^H u_c dy}{\int_{-H}^H dy} \quad (4)$$

The denominator of the above equation is $2H$. Under the assumptions of thermally and hydrodynamically fully developed laminar flow in a parallel plate channel, and neglecting viscous dissipation effect and heat generation, the final form of the energy equation can be expressed as follows:

$$(\rho C_p)_f u \frac{\partial T}{\partial x} = (\lambda(k_{\text{eff}} - k_f) + k_f) \frac{\partial^2 T}{\partial y^2} \quad (5)$$

where k_f and k_{eff} are the thermal conductivity of the fluid and the effective conductivity of the porous layer. The parameter λ is defined as

$$\begin{aligned} \lambda &= 0 & \text{for } \xi H \leq y < H \\ \lambda &= 1 & \text{for } -H \leq y \leq \xi H \end{aligned} \quad (6)$$

The boundary conditions for Eq. (5) can be written as

$$\begin{aligned} q'' &= k_f \left. \frac{\partial T_c}{\partial y} \right|_{y=H} = k_{\text{eff}} \left. \frac{\partial T_p}{\partial y} \right|_{y=-H} \\ T_c|_{y=\xi H} &= T_p|_{y=\xi H} \end{aligned} \quad (7)$$

Fluid enters the channel with temperature of T_i .

3.2 Solution Procedure

The solutions of dimensional differential equations with related boundary conditions are found by finite difference method by the help of MATLAB software. Finite difference forms of the equations and boundary conditions are written based on nodal difference rather than conservative flux at boundaries. The solution procedure starts with a given specific flow

rate and an assumed a negative pressure gradient value. The mean velocity is calculated by numerical solution of the momentum equations with using the assumed pressure value. The calculation continues until the mean velocity which is found numerically converges to the given specific flow rate. The energy equation is the second order partial difference equation, so a 2-dimensional domain is considered to obtain the solution of Eq. (5). The velocity distribution values obtained from the solution of momentum equation are used for the determination of temperature profile in the channel. Number of nodes for momentum equation is totally 101×1 , while for energy equation 101×301 nodes are used.

4 Dimensionless Study

The same channel shown in Fig. 1 is also considered for the dimensionless study. The dimensional form of heat and fluid flow equations are given by Eqs. (1), (2), and (5). The following dimensionless parameters are used to convert dimensional equations to the dimensionless form:

$$Y = \frac{y}{H}, M = \frac{\mu_{\text{eff}}}{\mu_f}, Da = \frac{K}{H^2}, G = -\frac{\partial P}{\partial x}, S = \frac{1}{\sqrt{MDa}},$$

$$U = \frac{\mu_f u}{GH^2}, T_{w\mu} = \frac{T_{wu} + T_{wl}}{2}, \theta = \frac{T - T_{w\mu}}{T_m - T_{w\mu}}, K^* = \frac{k_{\text{eff}}}{k_f} \quad (8)$$

where Da , M and S are Darcy number, viscosity ratio, and porous media shape parameter, respectively. After substituting the dimensionless parameters (8) into Eqs. (1) and (2), the following dimensionless form of these equations is obtained:

$$\frac{d^2 U_c}{dY^2} + 1 = 0$$

$$\frac{d^2 U_p}{dY^2} - S^2 U_p + \frac{1}{M} = 0 \quad (9)$$

where U_c and U_p are the dimensionless velocity of fluid at the clear and porous regions. The dimensionless forms of the boundary conditions Eq. (3) can also be obtained by the dimensionless parameters of Eq. (8).

$$U_c|_{Y=1} = U_p|_{Y=-1} = 0$$

$$\mu_f \left. \frac{dU_c}{dY} \right|_{Y=\xi} = \mu_{\text{eff}} \left. \frac{dU_p}{dY} \right|_{Y=\xi} \quad (10)$$

The solutions of Eq. (9) with boundary conditions given in Eq. (10) yield dimensionless velocity distribution equations for each region. The velocity distribution equation for clear region is found as

$$U_c = C_0 + C_1 Y + C_2 Y^2$$

$$C_0 = -\frac{2U_i - \xi + \xi^2}{2(-1 + \xi)}, C_1 = \frac{-1 + 2U_i + \xi + (-1 + \xi)\xi}{2(\xi - 1)}, C_2 = -\frac{1}{2} \quad (11)$$

where U_i is the interface velocity between porous layer and clear region. According to the solution of Eq. (9), the velocity distribution equation for porous region is found as

$$U_p = P_0 + P_1 \sinh\left(\frac{\xi - Y}{S}\right) + P_2 \sinh\left(\frac{Y + 1}{S}\right) \quad (12)$$

$$P_0 = \frac{S^2}{M}, P_1 = -\frac{S^2}{M \sinh\left(\frac{\xi+1}{S}\right)}, P_2 = \frac{MU_i - S^2}{M \sinh\left(\frac{\xi+1}{S}\right)}$$

Since shear stress is continuous at the interface (Eq. 10), the dimensionless velocity at the interface between porous and clear region (U_i) can be found as

$$U_i = \frac{S(-1 + \xi) \left(M(-1 + \xi) - 2S \tanh\left(\frac{1+\xi}{2S}\right) \right)}{2M \left(S - (-1 + \xi) \coth\left(\frac{1+\xi}{2S}\right) \right)} \quad (13)$$

The dimensionless form of the mean velocity of the fluid in the channel can be calculated as

$$u_{\text{mean}} = \frac{\int_{-H}^{\xi H} u_p dy + \int_{\xi H}^H u_c dy}{\int_{-H}^H dy} \Rightarrow U_{\text{mean}} = \frac{\int_{-1}^{\xi} U_p dY + \int_{\xi}^1 U_c dY}{2} \quad (14)$$

The solution of Eq. (14) along with Eqs. (11) and (12) gives:

$$U_{\text{mean}} = \frac{-M(6U_i + (-1 + \xi)^2)(-1 + \xi) + 12S^2(1 + \xi) + 24S(-2S^2 + MU_i) \sinh\left(\frac{1+\xi}{2S}\right)}{24M} \quad (15)$$

Finally, the dimensionless normalized velocity for each region can be determined as

$$\hat{u} = \frac{U}{U_{\text{mean}}} \quad (16)$$

In order to find dimensionless form of heat transfer equation for thermally and hydrodynamically fully developed flow, an overall thermal conductivity is defined:

$$k_m = \frac{(1 + \xi)k_{\text{eff}} + (1 - \xi)k_f}{2} \quad (17)$$

Thus, the overall Nusselt number for the considered problem can be defined as

$$Nu_m = \frac{h2H}{k_m} = \frac{2Hq''}{k_m(T_{w\mu} - T_m)} \quad (18)$$

At this point after some mathematical manipulation and by the definition of overall Nusselt number, two dimensionless heat transfer equation for clear flow region and for porous region can be found as

$$\frac{\partial^2 \theta_c}{\partial Y^2} + \frac{1}{2} \hat{u} Nu_m K_f^* = 0 \quad (19)$$

$$\frac{\partial^2 \theta_p}{\partial Y^2} + \frac{1}{2} \hat{u} Nu_m K_{\text{eff}}^* = 0 \quad (20)$$

where K_f^* and K_{eff}^* are k_m/k_f and k_m/k_{eff} , respectively. A parameter for specifying temperature at the boundary can be defined as

$$\beta = \frac{T_{\text{wl}} - T_{\text{wu}}}{2(T_m - T_{\text{w}\mu})} \quad (21)$$

Thus, the related boundary conditions can be written in terms of β

$$\begin{aligned} \theta_c|_{Y=1} &= -\beta \\ \theta_p|_{Y=-1} &= \beta \\ \theta_c|_{Y=\xi} &= \theta_p|_{Y=\xi} = \theta_i \end{aligned} \quad (22)$$

In the above boundary conditions, θ_i designates the dimensionless interface temperature of porous and clear region. When the dimensionless heat transfer equation for clear region (Eq. 19) with related boundary conditions (Eq. 22) is solved, the dimensionless temperature equation for clear region can be found:

$$\begin{aligned} \theta_c(Y) &= \frac{(y - \xi) \left(24B - K_f^* Nu_m (y-1) \left((\xi-1) \left(6C_0 + 2C_1 (y+1+\xi) + C_2 (1+y+y^2+\xi+y\xi+\xi^2) \right) \right) \right) + 24(y-1)\theta_i}{24(\xi-1)} \end{aligned} \quad (23)$$

where the coefficients C_0 , C_1 and C_2 are given in Eq. (11). The equation of dimensionless temperature in the porous region is found as

$$\begin{aligned} \theta_p(Y) &= \frac{1}{4(1+\xi)} \left(4\theta_i(1+Y) + (\xi-Y) \left(4B + K_{\text{eff}}^* Nu_m P_0(1+Y)(1+\xi) \right) \right. \\ &\quad + 2K_{\text{eff}}^* Nu_m S^2 \left((P_2 - P_1 Y + P_2 Y + P_1 \xi) \text{Sinh} \left(\frac{1+\xi}{S} \right) \right. \\ &\quad \left. \left. - (1+\xi) \left(P_1 \text{Sinh} \left(\frac{\xi-Y}{S} \right) + P_2 \text{Sinh} \left(\frac{1+Y}{S} \right) \right) \right) \right) \end{aligned} \quad (24)$$

Here, the coefficients P_0 , P_1 and P_2 are given in Eq. (12). If we want to investigate the distribution of dimensionless temperature throughout the channel according to Eqs. (23) and (24), the values of β , θ_i and Nu_m should be known. The following relations can be used to determine the values of β , θ_i and Nu_m

$$K^* \frac{\partial \theta_p}{\partial Y} \Big|_{Y=-1} = \frac{\partial \theta_c}{\partial Y} \Big|_{Y=1} \quad (25)$$

$$K^* \frac{\partial \theta_p}{\partial y} \Big|_{Y=\xi} = \frac{\partial \theta_c}{\partial y} \Big|_{Y=\xi} \quad (26)$$

$$\int_{-1}^1 \theta \hat{u} dY = 2 \quad \text{or} \quad \int_{-1}^{\xi} \theta_p \hat{u} dY + \int_{\xi}^1 \theta_c \hat{u} dY = 2 \quad (27)$$

Equation (25) is written based on the same heat flux at the walls of the channel, while Eq. (26) is written based on the continuous heat flux at the interface between clear fluid and porous medium. Finally, Eq. (27) is the compatibility equation which is written based on conservation of mass. The expressions for β , θ_i and Nu_m can be found by the above three relations:

$$\beta = -\frac{n_1(b_1 + b_2 t_1)}{B}, \theta_i = -\frac{n_1(t_1 + b_1 t_2)}{B} Nu_m = \frac{n_1(-1 + b_2 t_2)}{B}$$

where $B = -1 + n_3 t_1 + b_2(n_2 t_1 + t_2) + b_1(n_2 + n_3 t_2)$

(28)

where b_1 , b_2 , t_1 , t_2 , n_1 , n_2 , and n_3 are constants. These constants are too long and that is why they are not presented in this paper.

The definition of the individual Nusselt numbers for each wall can be expressed as

$$Nu_u = -\frac{2Hq''}{k_f(T_{wu} - T_m)} \quad \text{and} \quad Nu_u = \frac{h_u 2H}{k_f}$$

$$Nu_l = -\frac{2Hq''}{k_{\text{eff}}(T_{wl} - T_m)} \quad Nu_l = \frac{h_l 2H}{k_{\text{eff}}}$$
(29)

We can apply the conservation of energy onto each wall, which yields

$$h_u(T_m - T_{wu}) = k_f \frac{(T_m - T_{w\mu})}{H} \frac{\partial \theta_c}{\partial Y} \Big|_{Y=1}$$

$$h_l(T_m - T_{wl}) = k_{\text{eff}} \frac{(T_m - T_{w\mu})}{H} \frac{\partial \theta_p}{\partial Y} \Big|_{Y=-1}$$
(30)

After some algebra and by Eqs. (29), (30) and (21) (for the definition of β), the following relations can be obtained:

$$\frac{\partial \theta_c}{\partial Y} \Big|_{Y=1} = \frac{1}{2} Nu_u (1 + \beta)$$

$$\frac{\partial \theta_p}{\partial Y} \Big|_{Y=-1} = \frac{1}{2} Nu_l (1 - \beta)$$
(31)

The individual Nusselt numbers, Nu_u and Nu_l , can be found by solving Eqs. (30) and (31) along with Eqs. (23) and (24)

$$Nu_u = -\frac{24(\beta + \theta_i) + K_f^* Nu_m (\xi - 1)^2 (6C_0 + 3C_2 + (\xi + 2)(2C_1 + \xi C_2))}{12(1 + \beta)(\xi - 1)}$$

$$Nu_l = \frac{4(\beta - \theta_i) - K_{\text{eff}}^* Nu_m \left((\xi + 1)(P_0 - 2P_2 S + \xi P_0) + 2S \left(-P_1(\xi + 1) \text{Cosh} \left(\frac{\xi + 1}{S} \right) + (P_1 - P_2) S \text{Sinh} \left(\frac{\xi + 1}{S} \right) \right) \right)}{2(\beta - 1)(\xi + 1)}$$
(32)

The porous media in the channel results in the increment of pressure drop. First, the friction factor f should be defined. If we consider a channel which has the mean velocity of u_{mean} , the friction factor f for this channel can be written as

$$f = \frac{\left(-\frac{dP}{dx} \right) 2H}{\frac{1}{2} \rho u_{\text{mean}}^2}$$
(33)

According to the fully developed assumption, the flow has a constant negative pressure gradient $-dP/dx$ along the x -axis and this gradient is denoted by G , as defined in Eq. (8). Thus, f given by Eq. (33) becomes

$$f = \frac{4GH}{\rho u_{\text{mean}}^2}$$
(34)

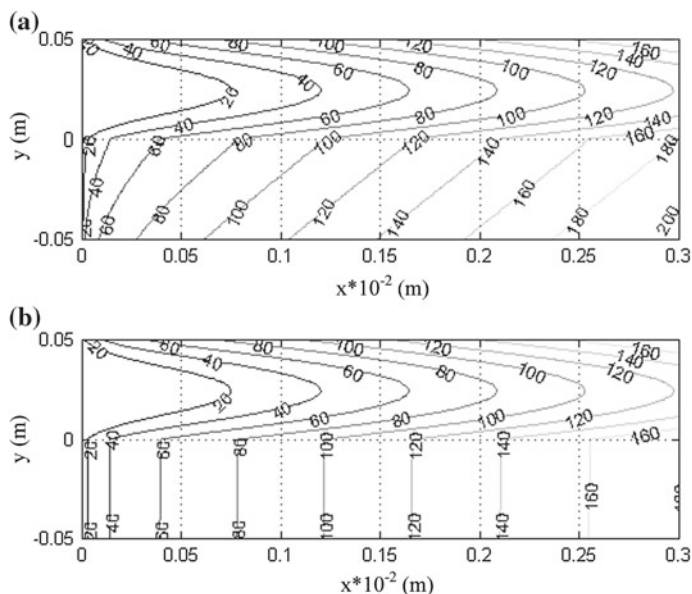


Fig. 2 Isotherm contours through the channel partially filled with porous medium: **a** glass particles, **b** aluminum alloy particles

Using the definition of the Reynolds number for the internal flow, the equation for the friction factor $f Re$ can have the following form

$$f Re = \frac{8}{U_{\text{mean}}} \quad (35)$$

where the mean velocity U_{mean} has been determined in Eq. (15). Thus, by Eq. (35), the friction factor for specified Reynolds number can be determined. The Reynolds number is defined as $Re = \rho U_{\text{mean}} 2H / \mu_f$ and it is macroscopic Reynolds number based on fluid velocity.

5 Results and Discussion

5.1 Dimensional Results

For the dimensional problem, a constant heat flux of 100 W/m^2 is imposed to the channel walls. The total height of the channel is taken as 0.1 m , while the length of channel 30 m . Half of the channel is filled with porous medium. The fluid in the channel is considered as air and it flows into the channel at 273 K . Figure 2a, b shows temperature distributions in the channel when the solid phase of the porous material are Glass and Aluminum Alloy with thermal conductivity of 1.1 and 120 W/mK , respectively. The porosity of the porous medium is considered as 0.86 and consequently viscosity ratio is found as $\mu_{\text{eff}} / \mu_f = 1.16$. The permeability of porous layer is taken as $6.02 \times 10^{-7} \text{ m}^2$. For the channel with Al solids, effective thermal conductivity is greater than the channel with glass material. Thus, almost a uniform temperature distribution is observed in the porous layer (Figure 2b). For the channel with glass solids, the temperature at the wall on which porous layer is located is greater than temperature of wall has contact with clear fluid due to higher thermal conductivity in

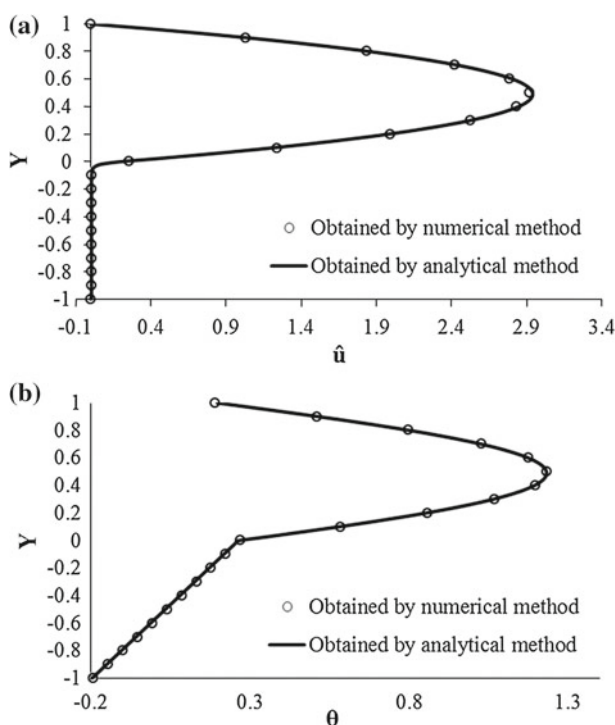


Fig. 3 The comparison between results of the analytical and numerical approaches: **a** normalized velocity (\hat{u}), **b** dimensionless temperature (θ)

the porous layer. It should be mentioned that only the outlet temperature profile of channel, obtained numerically, is used in this study. The obtained outlet temperature profile represents the fully developed temperature profile and it is used for validation of the analytical results.

5.2 Comparison of Dimensional and Dimensionless Results

The velocity and temperature distribution in the channel with different permeability and solid materials (glass and num alloy) are found numerically. The attention focused at the outlet of the channel in which heat and fluid flows are fully developed. The temperature and velocity profiles at the outlet of the channel are converted to the dimensionless forms using defined dimensionless parameters of Eq. (8). The converted results are compared with the results from the solutions of the analytical expressions. In this section, a sample of the performed comparisons is shown. Figure 3a shows comparison of normalized velocities obtained from dimensionless (analytical solution) and converted dimensional velocity profiles (numerical solution) for a channel which has permeability of $6.02 \times 10^{-7} \text{ m}^2$. Figure 3b indicates the dimensionless temperature profile of the same channel when the material of the solid in the filled region is glass. As seen from Fig. 3a, b, the numerical results obtained from solution of dimensional form of the governing equations are consistent with the analytical results achieved from the dimensionless form of the governing equations.

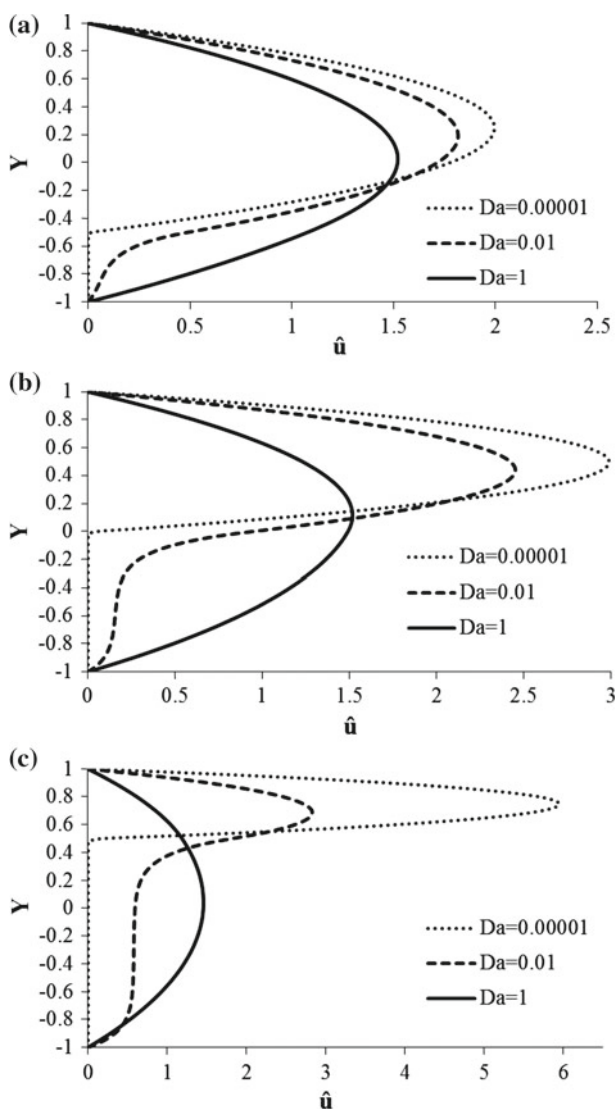


Fig. 4 The effect of porous layer thickness on the normalized velocity (\hat{u}) for different values of Da : **a** $\xi = -0.5$, **b** $\xi = 0$, **c** $\xi = 0.5$

5.3 Effects of Da , ξ , and K^*

The effects of the Darcy number Da and the porous thickness ξ on normalized velocity profiles \hat{u} can be seen in Fig. 4. Figure 4a illustrates the variation of \hat{u} for different values of Da when $\xi = -0.5$. For $Da = 1$, which means almost completely clear fluid channel, the normalized velocity profiles are symmetric. As seen, the normalized velocity in porous layer \hat{u} is slower than the normalized velocity in clear fluid layer for $Da = 0.01$. As Da decreases, the fluid is squeezed out from the porous medium to the clear fluid layer due to the strong resistance of the obstacles in the porous layer. That is why the velocity in the clear fluid region

(upper part of the channel) is greater than fluid velocity in the porous layer region (lower part) of the channel. The maximum velocity \hat{u}_{\max} occurs in the clear fluid region and it is increased by both decreasing Da and/or increasing thickness of the porous layer ξ . Figure 4b depicts the normalized velocity \hat{u} when the bottom half of the channel is filled with porous medium ($\xi = 0$). By increasing ξ , the air flow rate in the clear region increases and \hat{u}_{\max} increases compared to the channel with $\xi = -0.5$. The normalized velocity distributions \hat{u} for different values of Da when $\xi = 0.5$ are shown in Fig. 4c. As expected, the maximum value of \hat{u} becomes greater due to the narrowness of the clear fluid region.

Figure 5 demonstrates dimensionless temperature distributions θ in the channel with different values of Da and K^* when $\xi = 0$. It should be mentioned that the value of θ is defined based on the average of wall temperatures given in Eq. (8). The variation of θ is presented to have an idea how varies θ with Da and thermal conductivity ratio K^* . Figure 5a shows the θ profile when $K^* = 0.01$ for which thermal conductivity of fluid K_f^* is very higher than effective thermal conductivity of porous media K_{eff}^* . For all plotted values of Da , the dimensionless temperatures θ are almost uniform in the clear fluid region ($\xi = 0$). Figure 5a also shows that when Da increases, θ increases for the both of clear fluid and porous layer regions. Figure 5b shows the variation of θ for same channel when $K^* = 1$, which means that k_{eff} equals to the fluid thermal conductivity k_f . That is why a symmetrical behavior of θ is observed for $Da = 1$. The maximum of θ is shifted to the clear fluid region by the decrease of Da since flow rate in the porous layer is reduced. Figure 5c indicates profiles of θ for $K^* = 100$, which means that the effective thermal conductivity of porous layer is considerably greater than the fluid thermal conductivity. There is almost a uniform distribution of θ in the porous region. The values of θ for porous region increases with increasing Da since the fluid can flow easier in the porous layer.

Figure 6 illustrates the variation of the overall Nusselt number Nu_m with thermal conductivity ratio K^* for three different values of Da when $\xi = 0$. For considered three values of Da ($Da = 0.0001$, 0.005 and 0.1), the values of Nu_m at $K^* = 0.01$ and 100 are very small and almost equal. For $K^* = 0.01$ or $K^* = 100$, one wall of the channel is in contact with a very low thermal conductive material. That is why heat transfer coefficient from one wall to the fluid is very smaller than the heat transfer coefficient of another wall to the adjacent fluid. Consequently, this causes the decrease of overall heat transfer coefficient. However, for K^* around 1, the overall Nusselt number Nu_m takes a maximum value. For the channels with $K^* = 1$, heat transfer coefficient for both walls of the channel is the same and heat easily flows from both walls to the fluid. By the increase of Da , the overall Nusselt number Nu_m increases since flow resistance in lower side of the region of channel is reduced.

Figure 7 indicates the change of Nu_m with the porous layer thickness ξ for three different values of K^* as 0.01, 1, and 100 when $Da = 0.0001$. As expected, maximum Nu_m belongs to the channel with porous layer of $K^* = 1$. It is seen that Nu_m slightly decreases by increasing the porous layer thickness, ξ since the flow resistance in the channel increases. The increase of ξ leads to the increase of the flow rate in the clear fluid region and consequently heat transfer coefficient in the fluid region increases. That is why, after $\xi = 0.7$, the increase of ξ causes the increase of Nu_m . For the channel with thermal conductivity ratio $K^* = 100$, the increase of ξ leads to an increase of Nu_m since k_{eff} is highly greater than k_f . The change of Nu_m with ξ for a channel with $K^* = 0.01$ is similar to that of the channel with $K^* = 1$. The increase of ξ in a channel in which porous layer has lower thermal conductivity compared to the clear fluid, reduces Nu_m . However, after a porous layer thickness around $\xi = 0.7$, the velocity in the clear fluid region increases considerably and that is why Nu_m increases.

The variation of the individual Nusselt numbers Nu_u and Nu_l for the upper and lower walls with Da for different values of K^* when $\xi = 0$ can be seen in Fig. 8. This figure shows

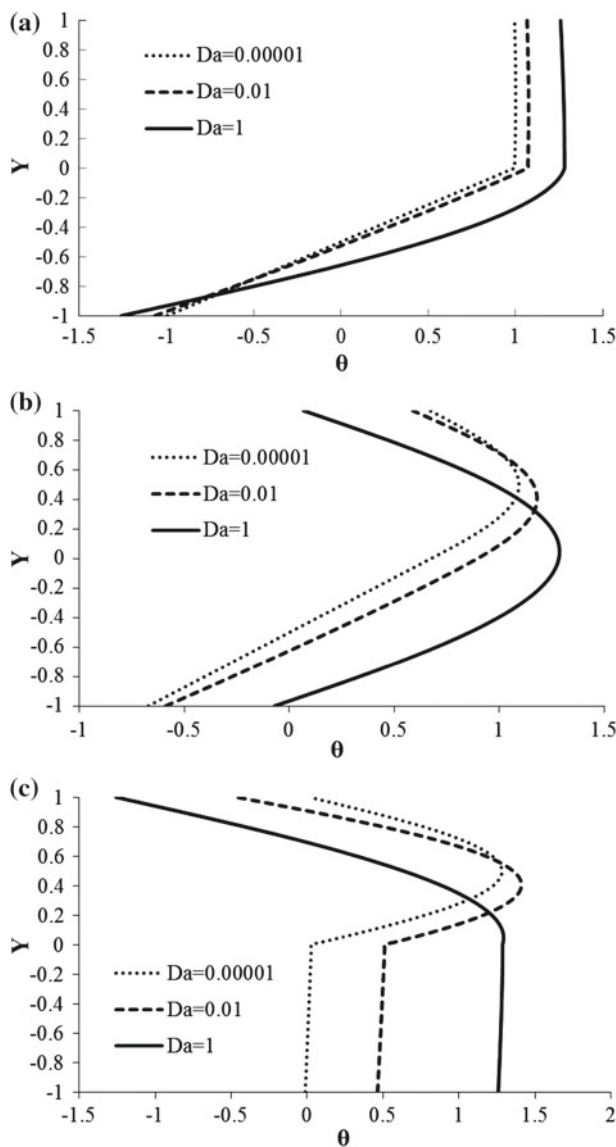


Fig. 5 Dimensionless temperature distributions (θ) for the flows with different values of Da and K^* when $\xi = 0$: **a** $K^* = 0.01$, **b** $K^* = 1$, **c** $K^* = 100$

that the individual Nusselt numbers for upper wall (Nu_u) slightly decreases with Da when $K^* = 1$ and 100 since by increasing Da the flow rate in the clear fluid region decreases. The change of Nu_u with Da for $K^* = 0.01$ is completely different than for $K^* = 1$ and 100 . There is a discontinuity in the individual Nusselt number for the upper wall and for Da around 0.001 for the channel with $K^* = 0.01$. The change of the sign of Nu_u does not mean that heat transfer direction is changed at the upper wall. For the region with $Da < 0.001$, the wall temperature of the upper wall T_{wu} is greater than the mean temperature T_m in the

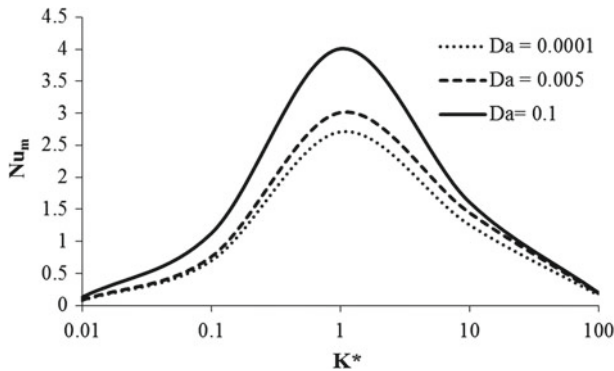


Fig. 6 The change of the overall Nusselt number (Nu_m) with K^* for different values of Da when $\xi = 0$

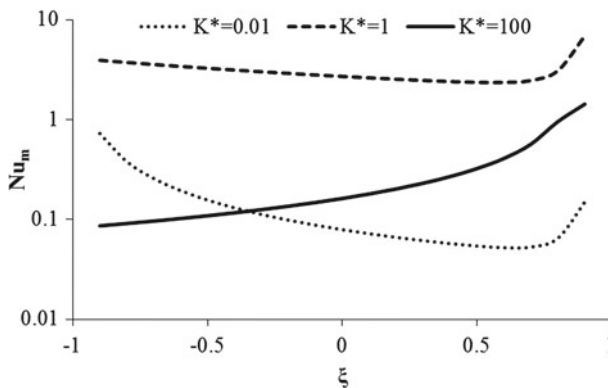


Fig. 7 The change of overall Nusselt number (Nu_m) with the porous layer thickness ξ for different values of K^* when $Da = 10^{-4}$

channel and that is why individual Nusselt number is positive. By increase of Da , the value of T_{wu} becomes smaller than T_m the mean temperature in the channel and Nu_u takes negative values. Figure 8b shows that the change of individual Nusselt number for the lower wall of the channel with Da for the same thermal conductivity ratios K^* . The increase of Da causes the increase of Nu_l for $K^* = 0.01$ and 1, since fluid with high thermal conductivity, flowing in the clear fluid region, enters to the porous layer. For $K^* = 100$, again a discontinuity in Nu_l is observed. The value of T_{wl} is greater than T_m for the region with $Da < 0.01$. However, by the increase of Da in the region of $Da > 0.01$, T_{wl} becomes less than T_m and the sign of the Nu_l is changed. Again, this change of Nu_l should not be commented as the change of heat flux at the boundaries.

The variation of the friction coefficient $f Re$ with Da for three values of the porous layer thickness ξ can be seen in Fig. 9. It is seen that the value of $f Re$ for $\xi = -0.5$ is smaller than the friction coefficient for $\xi = 0$ and 0.5. This is an expected result since the porous layer is thinner compared to $f Re$ of $\xi = 0$ and 0.5. By an increase of ξ , particularly after $\xi = 0$, the values of $f Re$ increases. Moreover, by the increase of Da and decrease of flow resistance ξ , the friction coefficient $f Re$ also decreases. A dramatic decrease of $f Re$ with the increase

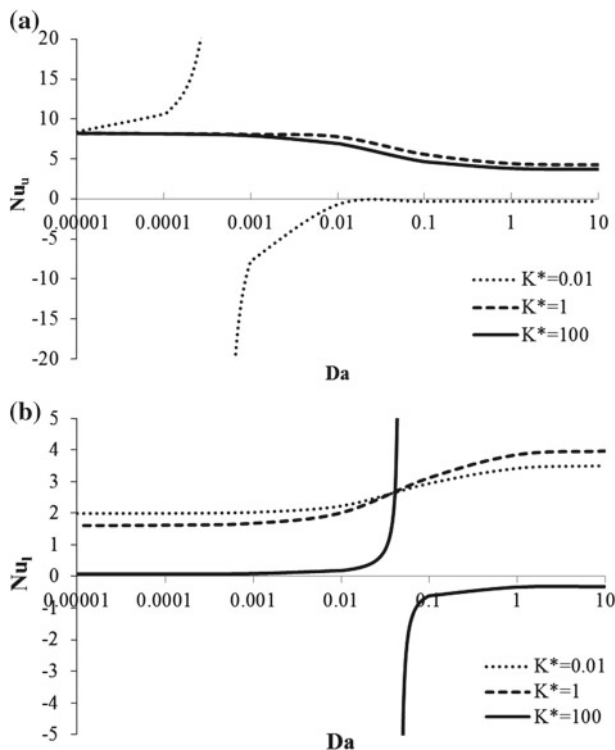


Fig. 8 Variation of the individual Nusselt number with Da and K^* when $\xi = 0$: **a** Nusselt number for the upper wall (Nu_u), **b** Nusselt number for the lower wall (Nu_l)

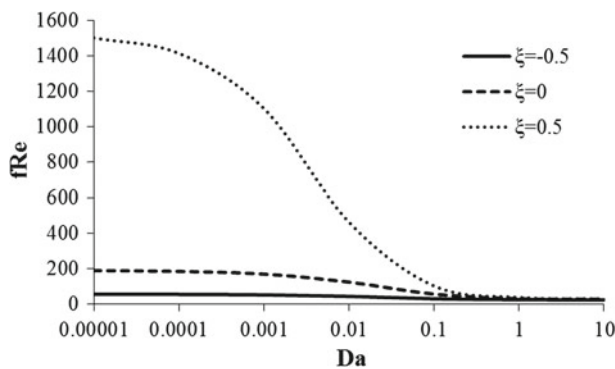


Fig. 9 The change of the friction coefficient ($f Re$) with Da for different values of ξ

of Da is observed for the channel with $\xi = 0.5$. For high values of Da (i.e., $Da = 1$), the friction coefficient $f Re$ becomes independent from ξ since the flow approaches that of a clear channel.

6 Conclusion

The present theoretical study is carried out for forced convection between two parallel plates channel partially filled with porous media. A constant heat flux is imposed to the upper and lower walls of channel. The Brinkman-Darcy model was used to model the flow inside the porous layer. The dimensional governing equations are solved numerically, while the dimensionless governing equations are solved analytically. The results of two approaches are compared with each other and excellent agreement is observed. Based on the obtained results, following remarks can be concluded:

- Velocity profile is highly influenced from porous layer thickness. By increase of porous layer thickness, velocity in clear fluid region increases. Moreover, the increase of porous layer thickness increases pressure drop in the channel, dramatically.
- The overall Nusselt number takes maximum value for $K^* = 1$. By the increase of the Darcy number, Da , the maximum value of the overall Nusselt number increases.
- For the channel with $K^* = 1$ and 0.01, the overall Nusselt number Nu_m decreases with the increase of porous layer thickness up to $\xi = 0.75$. After these values of the porous layer thickness, the overall Nusselt number Nu_m increases with ξ .
- For the channel with $K^* = 100$, the overall Nusselt number Nu_m increases with the increase of ξ for the whole region of the porous layer thickness.
- For specific values of thermal conductivity ratio, K^* , there is a discontinuity in the change of the individual Nusselt numbers with Da . The upper wall Nusselt number Nu_u takes the infinity value around $Da = 0.0005$ when $K^* = 0.01$. Similarly, the lower wall Nusselt number Nu_l takes infinity value around $Da = 0.05$ when $K^* = 100$.
- The change of the sign of the individual Nusselt number is due to the change of the sign of the wall and mean temperature differences.

References

- Al-Nimr, M.A., Alkam, M.K.: A modified tubeless solar collector partially filled with porous substrate. *Renew. Energy* **13**, 165–173 (1997)
- Forooghi, P., Abkar, M., Saffar-Avval, M.: Steady and unsteady heat transfer in a channel partially filled with porous media under thermal non-equilibrium condition. *Transp. Porous Media* **86**, 177–198 (2010)
- Guo, Z., Kim, S.Y., Sung, H.J.: Pulsating flow and heat transfer in a pipe partially filled with a porous medium. *Int. J. Heat Mass Transf.* **40**, 4209–4218 (1997)
- Jen, T.-C., Yan, T.Z.: Developing fluid flow and heat transfer in a channel partially filled with porous medium. *Int. J. Heat Mass Transf.* **48**, 3995–4009 (2005)
- Kuznetsov, A.V.: Analytical investigation of couette flow in a composite channel partially filled with a porous medium and partially with a clear fluid. *Int. J. Heat Mass Transf.* **41**, 2556–2560 (1998)
- Kuznetsov, A.V.: Fluid flow and heat transfer analysis of Couette flow in a composite duct. *Acta Mechanica* **140**, 163–170 (1999)
- Kuznetsov, A.V., Nield, D.A.: Forced convection in a channel partly occupied by a bidisperse porous medium: asymmetric case. *Int. J. Heat Mass Transf.* **53**, 5167–5175 (2010)
- Mohamad, A.A.: Heat transfer enhancements in heat exchangers fitted with porous media part I: constant wall temperature. *Int. J. Thermal Sci.* **42**, 385–395 (2003)
- Morosuk, T.V.: Entropy generation in conduits filled with porous medium totally and partially. *Int. J. Heat Mass Transf.* **48**, 2548–2560 (2005)
- Nield, D.A., Kuznetsov, A.V.: Forced convection in a channel partly occupied by a bidisperse porous medium: symmetric case. *ASME J. Heat Transf.* **133**, 072601 (2011)
- Poulikakos, D., Kazmierczak, M.: Forced convection in a duct partially filled with a porous material. *ASME J. Heat Transf.* **109**, 653–662 (1987)
- Satyamurty, V.V., Bhargavi, D.: Forced convection in thermally developing region of a channel partially filled with a porous material and optimal porous fraction. *Int. J. Thermal Sci.* **49**, 319–332 (2010)

- Sayehvand, H., Shokouhmand, H.: Study of forced convection in a pipe partially filled with a porous medium. The 4th Wseas International Conference on Heat Transfer, Thermal Engineering and Environment, pp. 292–300. Elounda (2006)
- Shokouhmand, H., Jam, F., Salimpour, M.R.: The effect of porous insert position on the enhanced heat transfer in partially filled channels. *Int. Commun. Heat Mass Transf.* **38**, 1162–1167 (2011)
- Teamah, M.A., El-Maghlany, W.M., Khairat Dawood, M.M.: Numerical simulation of laminar forced convection in horizontal pipe partially or completely filled with porous material. *Int. J. Thermal Sci.* **50**, 1512–1522 (2011)
- Yang, C., Liu, W., Nakayama, A.: Forced convective heat transfer enhancement in a tube with its core partially filled with a porous medium. *Open Transport Phenom. J.* **1**, 1–6 (2009)
- Yang, C., Nakayama, A., Liu, W.: Heat transfer performance assessment for forced convection in a tube partially filled with a porous medium. *Int. J. Thermal Sci.* **54**, 98–108 (2012)